Review

Shale Oil Occurrence Mechanisms: A Comprehensive Review of the Occurrence State, Occurrence Space, and Movability of Shale Oil

Yangbo Lu [1], Feng Yang [1,2,*], Ting'an Bai [1], Bing Han [3], Yongchao Lu [1] and Han Gao [4]

[1] Key Laboratory of Theory and Technology of Petroleum Exploration and Development in Hubei Province, China University of Geosciences, Wuhan 430074, China

[2] Key Laboratory of Petroleum Resources Research, Gansu Province, Lanzhou 730000, China

[3] Inner Monglia Key Laboratory of Magmatic Mineralization and Ore-Prospecting, Hohhot 010020, China

[4] No. 11 Production Factory of Changqing Oilfield Company, PetroChina Co., Ltd., Qingyang 745000, China

* Correspondence: fengyang@cug.edu.cn

Abstract: Shale oil resources are important supplements for the gradually decreasing oil production from conventional reservoirs. Although the exploitation and development of shale oil have achieved considerable progress in the last decade, the commercial extraction of hydrocarbons from shales is still difficult, especially in the lacustrine sedimentary basins of China. One of the key points controlling the successful extraction of hydrocarbons from shale systems is the understanding of the occurrence mechanism of shale oil. This study comprehensively summarizes the theories and techniques to characterize oil occurrence state, occurrence space, oil content, and oil movability in shale systems. Sophisticated instruments, such as high-resolution scanning electron microscopy and high-energy ray imaging, were utilized to qualitatively analyze the pore networks of shales. Advanced physical experiments and numerical simulation techniques, including step-by-step rock pyrolysis, solvent extraction, and NMR, were introduced to characterize shale oil adsorption and movability. By the comparative analysis of the occurrence space, it is found that the image observation technique especially focuses on concentrated pores, such as organic matter-hosted pores. The fluid injection technology yields particular pore size information, which should be calibrated using other information. The 3D digital core, demonstrating the spatial distribution of minerals and pores, is an effective input for shale oil flow simulation. Geological controls analysis about oil retention in organic-rich shales has found that the inorganic matter pores and fractures are probably the "sweet spot" of shale oil, due to the low oil adsorption and high light hydrocarbons content. Many physical experiments measure the total free oil content but neglect the hydrocarbon–rock interaction and the sequential migration of hydrocarbon compounds. Thus, micro-scaled experiments measuring the hydrocarbon adhesion forces are needed to uncover the occurrence mechanism of shale oil in the future.

Keywords: shale oil; occurrence space; occurrence state; movability; oil retention

1. Introduction

One of the most significant achievements in fossil fuels in the last decade is the commercial extraction of hydrocarbons from unconventional shale reservoirs. In 2019, the total crude oil production in the U.S. reached 609 million tons, of which 65% was produced from tight shales [1]. Crude oil production has doubled since 2010 in the U.S., primarily driven by the effective development of tight shale systems using horizontal drilling and hydraulic fracturing. In fact, shale systems have been ignored for a long time, and regarded only as source rocks of hydrocarbons throughout history. The retained hydrocarbons in shales were unappreciated until advanced drilling and completion technologies were applied to economically extract oil and gas [2]. Currently, unconventional shales have

received new attention in petroleum generation, retention, migration, and accumulation for academic and industrial researchers around the world.

The effective developments of liquid hydrocarbons have been successfully achieved in a lot of shale systems in North America, including the Wolfcamp shales in the Permian Basin [3], Eagle Ford shales in southern Texas [4], Bakken shale formations in the Williston Basin [5], etc. Shale oil formations in North America were mainly deposited in marine sedimentary basins. The organic matter of these shales is at a high thermal maturity stage. These shales are also characterized by high light hydrocarbons content and movable oil content. Meanwhile, there are also considerable shale oil resources in China, including the Triassic Yanchang Formation in the Ordos Basin [6], the Cretaceous Qingshankou Formation in the Songliao Basin [7], the Permian Lucaogou Formation in the Santanghu Basin, and the Palaeogene Shahejie Formation in Bohai Bay Basin [8], etc. Unlike the marine sedimentary basins, shale oil formations in China were mainly deposited in lacustrine sedimentary environments [9]. Lacustrine shales are characterized as strongly heterogeneous in fabric, texture, and mineralogy. Shale oil extracted from the lacustrine source rocks commonly contains more asphaltene and resin content [10]. Thus, lacustrine shale oil is less movable compared to shales from marine sedimentary basins. Operators drilled many wells in lacustrine shale formations but did not always achieve satisfactory results. For example, the initial yield of the BY1 well, drilled in the first demonstration plot of China, was about 8.22 m^3/d after hydraulic fracturing and quickly decreased to 1.6 m^3/d [11]. Oil production from the HF1 well, drilled in the first breakthrough plot of lacustrine shale oil in China, was 23.6 m^3/d initially and soon decreased to about 1 m^3/d [12]. Thus, the effective development of shale oil in China is fairly difficult considering the severe reservoir heterogeneity and low flow ability of hydrocarbons [13]. The limited production of lacustrine shale oil is probably related to the poor understanding of petroleum generation and retention in shale systems [14].

Compared to conventional reservoirs, shales are much tighter with low porosity and ultra-low permeability. Minerals in shales, including organic matter and inorganic matter, are much more fine-grained and diversified. Shale systems are further complicated by the diagenetic transformation of inorganic minerals and hydrocarbons generated from organic matter [14]. Furthermore, the particle size and pores of shales are extremely fine [15]. Consequently, the hydrocarbon generation, expulsion, and retention are significantly different from the conventional reservoirs. Many characterization technologies used in sandstones and carbonates are not applicable to shales [16]. It is challenging to accurately estimate the pore structure, oil content, and oil movability of shale systems.

Previous investigations about shale oil have found that shale oil enrichment in lacustrine basins is affected by the lithofacies, minerals, interlayers, reservoir characteristics (pores, porosity, permeability, fractures), and organic geochemistry properties [17–19]. In lacustrine shale systems, laminated shales are thought to be favorable for shale oil accumulation [17]. Liu et al. thought that the laminated siliceous mudstones with moderate total organic carbon (TOC) content have abundant reservoir space and are the most favorable lithofacies for shale oil enrichment [18]. Bai et al. investigated the lacustrine shale oil accumulation in the Bohai Bay Basin and found that the interparticle pores in carbonates act as the reservoir spaces of shale oil [19]. Hu et al. thought that fractures provide oil migration pathways from source rocks to the reservoir, thus the interbedded intervals with abundant fractures are favorable for shale oil accumulation [20]. The fluid movability, abnormal fluid pressure, interlayers, and developed fractures are important to the high production of shale oil. In terms of the occurrence mechanism, molecular simulations have been adopted to analyze the adsorption behavior of shale oil at a micro-scale [21]. The occurrence space of shale oil can be observed by direct imaging techniques. Indirect methods, including nuclear magnetic resonance (NMR) and pyrolysis experiments, are also applied to investigate the occurrence state and content of shale oil [22–24]. Rock pyrolysis experiments divide hydrocarbons in shales into free oil and pyrolytic hydrocarbons, taking 300 °C as the boundary [22]. However, several researchers argued that a certain amount of

free oil was considered as pyrolytic hydrocarbons in the pyrolysis experiments [23]. Shale oil is recognized as adsorption, free, and miscible states (dissolved states) using NMR [24]. However, the geological controls on shale oil content and movability are still not clear.

Although researchers have tried to estimate shale oil content and movability from the perspective of experiments and numerical simulations, the analyzed results using different technologies are not always consistent. In particular, the evaluation of shale oil movability is a little chaotic. Many researchers focus on measuring the total free oil content. However, these macro-scaled measurements commonly neglect the intrinsic interactions between hydrocarbons and rock. The purposes of this paper are to summarize the theories and techniques to characterize the occurrence state, occurrence space, oil content, and oil movability of shale systems. Geological controls for oil retention in organic-rich shales were also discussed. This paper comprehensively analyzes various evaluation methods and their limitations for shale oil occurrence and storage. It also conducts a preliminary analysis of the interactions between hydrocarbons and rock, which provides insight into the understanding of the occurrence mechanism of shale oil at a micro-scaled level.

2. The Geological Definition of Shale Oil

2.1. Definition of Shale Oil

Shale oil refers to the non-gaseous hydrocarbons stored in organic-rich shales, mudstones, and their thin interlayers (siltstones, carbonates, etc.) [25]. During the early stage, the definition of shale oil was disputed by many researchers from a couple of different perspectives, including sedimentary lithology, reservoir space, and organic matter characteristics, etc. [26]. The initial definition of shale oil only refers to the oil accumulated in the organic-rich shales and mudstones with self-generated and self-stored characteristics. With the development of unconventional reservoirs, researchers and operators have loosened the definition: shale oil contains the petroleum not only retained in shales but also stored in interlayered tight sandstones and carbonate. In other words, petroleum accumulated in both self-generated self-stored reservoirs and short-distance migrated reservoirs can be ascribed to shale oil. In the "geological evaluation method for shale oil" (GB/T38718-2020) formulated by the standardization administration of China in 2020 [27], shale oil refers to oil stored in organic-rich shale systems with a thickness of fewer than 5 m for each organic-lean interbedded layer and a ratio of less than 30% for the accumulated thickness of the interbedded layers.

2.2. The Occurrence State of Shale Oil

Oil stores in organic-rich shale systems via free, adsorption, and absorption (solvation) states [28]. Free shale oil mainly stores within interlayered fractures, structural fractures, and overpressured fractures [29]. It also occurs as a free state in the recrystallized intercrystalline pores and dissolution-related pores with large pore diameters and forms locally continuous hydrocarbon aggregation [30]. Adsorbed shale oil is mainly associated with organic matter and clay minerals. Because of the van der Waals force and Coulomb force between these minerals and hydrocarbon molecules, oil in the adsorbed state presents with a solid-like form for which flow is difficult [31]. The absorption state of shale oil is that shale oil is dissolved in kerogen, which causes the kerogen to expand.

3. Occurrence Space Characterization of Shale Oil

Shale systems are severely heterogeneous. Figure 1 illustrates the mineral compositions of Barnett shale from Fort Worth Basin [30] and Chang 7 shale from Ordos Basin [6]. There is significant variation in mineral compositions of shales, even from the same formation. Shale oil movability is closely related to the minerals, pore structure, pore size distribution, and pore connectivity.
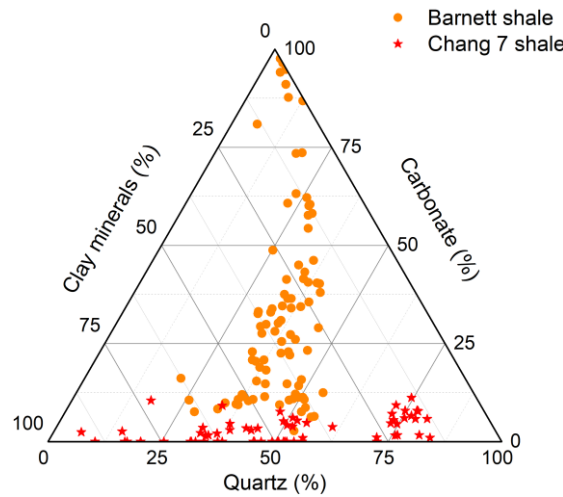
Figure 1. Mineral compositions of Barnett shale from Fort Worth Basin [30] and Chang 7 shale from Ordos Basin [6].

There are several types of micropores and nanopores in shale reservoirs, including organic matter-hosted pores, intergranular pores, dissolution-related pores, and microfractures [32]. Recently, many advanced technologies have been introduced to qualitatively and quantitatively characterize the occurrence space of shale oil. These techniques can be mainly classified into three categories: image observation method, fluid injection method, and high-energy ray method (Figure 2).
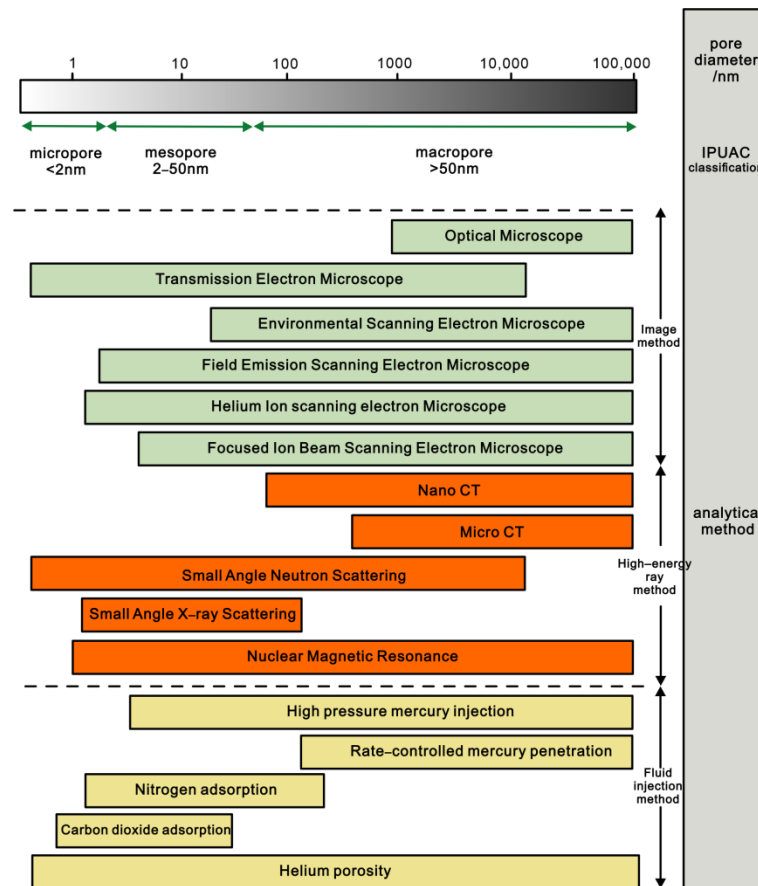

Figure 2. Experimental methods used to characterize the pore structure of shales.

3.1. Image Observation Technology

Image observation is a kind of technology that uses high-resolution imaging technology to directly observe the microscopic pore characteristics of shales. Using advanced imaging instruments, including focused ion beam-scanning electron microscopy (FIB-SEM), field emission-scanning electron microscopy (FE-SEM), atomic force microscopy (AFM), scanning transmission electron microscopy (STEM), helium ion-scanning electron microscopy (HIM), etc., the geometrical morphology of nano-scaled pores in shales can be visually observed. Generally, samples are mechanically polished before image observation. However, the cutting force during mechanical polishing may produce artificial fractures and pores. The abrasive particles used in mechanical polishing also easily occlude pores. Thus, shale samples prepared by mechanical polishing are not always satisfactory for image observation. In order to produce smooth and flat surfaces, Loucks et al. [32] utilized argon ion polishing technology in a metal surface treatment to prepare shale samples and obtained a high-quality sample surface. Combined with scanning electron microscopy, types of nano-scaled pores in organic matter of shales were observed [33–35]. Subsequently, argon ion polishing technology has been widely used to prepare shale samples.

For the conventional reservoirs, an optical microscope is feasible to observe their pore structure, with pore diameters being one micrometer or larger. However, the resolution of optical microscopes (about 0.01mm) is not high enough to observe the mineral arrangements and pore morphology of shales. Field emission-scanning electron microscopy (FE-SEM) can acquire images with a high resolution of up to 5 nm. After argon ion polishing, the samples are coated with gold or carbon to increase the conductivity and then used for FE-SEM imaging (Figure 3, [36]). Mastalerz et al. [37] studied the effect of argon ion polishing on shale samples during sample preparation and believed that the organic matter thermal alteration usually involves the volatilization of light hydrocarbon components. Thus, more care should be taken during the polishing of immature samples and oil window samples. With the application of FE-SEM, Wang et al. [38] investigated the pore structure of lacustrine shales in the Ordos Basin and found that hydrocarbon generation, mineral transformation, and compaction affected the evolution of pores.
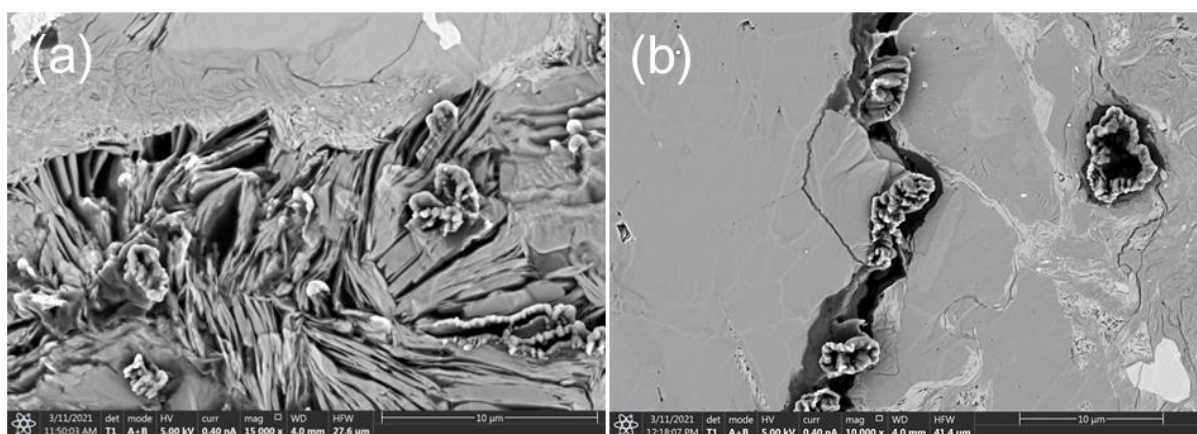
Figure 3. FE-SEM images showing moveable oil spilling from (**a**) interparticle pores of clay minerals (modified from Zheng et al. [36]); (**b**) microfracture of shales in the Ordos Basin.

Scanning transmission electron microscopy (STEM) scans the sample surface using electron beams and images by electron penetration. Laura constructed the three-dimensional (3D) structure of shales using STEM tomography and found that the nano-scaled pores below 20nm dominate in number but do not form connected pore networks, while the pores with pore sizes between 20nm and 60nm are well connected and therefore controlled the transport property of shales [39].

Focused ion beam-scanning electron microscopy (FIB-SEM) accelerates the ion beam generated by liquid metal (most FIB uses Ga) ion source through an ion gun and strips the

surface atoms to complete the micro- and nano-scaled surface topography. Combined with the computer algorithms, FIB-SEM presents the 3D distribution of pores and quantitatively provides the pore structure parameters and pore connectivity [40]. Zhou et al. [41] used FIB-SEM to study the two-dimensional and three-dimensional characteristics of shales from the Longmaxi Formation and calculated pore size distributions of the three-dimensional (3D) digital rock reconstructed from 600 consecutive FIB-SEM images.

Helium ion microscopy (HIM) is a method of imaging samples by accelerating and concentrating helium beams in the sample surface. Compared with electron beams, helium ion beams can better detect the internal structural characteristics of small pores; due to that, coating before electron microscope observation may destroy fine pores. HIM can obtain more reliable images of pores by direct observation without coating. Huang et al. used HIM to study the formation and evolution of organic matter pores in shales [42]. They divided the formation process of organic matter pores into four stages: formation, expansion, connection, and consolidation. King et al. found that organic matter contains an anomalous population of pores of the order ~2 nm [43]. They thought that these narrow pores were produced when the excess internal pressure failed to create escape pathways for the generated fluids during the kerogen diagenesis process.

Atomic force microscopy (AFM) is a scanning probe technology that approaches the sample surface with a highly sensitive probe installed on the cantilever. The interaction force between the needle tip of the probe and the sample surface deforms the cantilever beam. Using the optical leverage principle, the small deformation of the cantilever beam is amplified and converted into electrical signals so as to obtain the surface morphology and roughness information of the sample. The AFM not only produces high-resolution 2D and 3D images, but also characterizes the mechanical properties of the sample, such as Young's modulus, adhesion force, and electric potential (Figure 4). Javapour et al. [44] used AFM to characterize the surface topography of shales, especially the nano-pore characteristics of shale surfaces. Tian et al. [45] studied the kerogen and minerals in shales using AFM with the PeakForce Tapping mode and reported that the adhesion decreased in the order: kerogen > illite > montmorillonite > calcite > muscovite. Bai et al. [46] found that surface roughness affects the adhesion of shale: the higher the surface roughness, the greater the adhesion force. Wang et al. [47] characterized the organic matter of shales by atomic force microscopy combined with infrared spectroscopy (AFM-IR) and obtained the distribution of functional groups of organic matter.
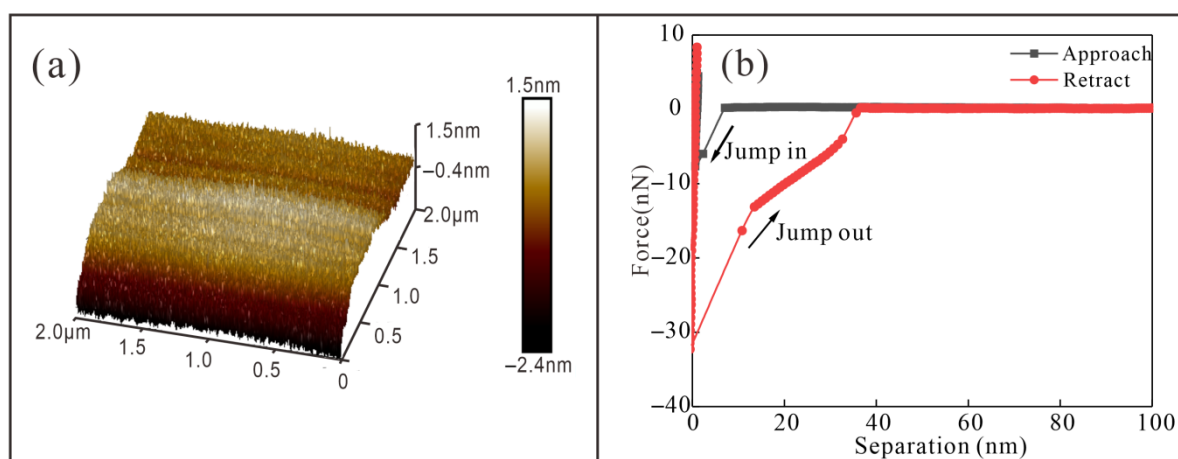
Figure 4. (**a**) Pore surface of mica scanning by AFM; (**b**) The adhesion force curves of shale oil on mica surface detect by AFM (modified from Bai et al. [46]).

3.2. Fluid Injection Technology

The fluid injection technique quantitatively characterizes pore structure by injecting fluids that do not react with the minerals of the samples. By precisely recording the amount

of injected fluid during the fluid intrusion and extrusion processes, the pore structure parameters can be estimated based on the hypothetical models. This experiment is easy to perform on various porous media, whether regular or irregular. Thus, it is one of the most widely-used techniques in characterizing the pore structure of materials. According to the injected fluids, this kind of technique mainly includes mercury intrusion porosimetry (MIP), nitrogen adsorption, carbon dioxide adsorption, helium injection, etc.

The MIP technique records the injection pressure values and the volume of mercury intrusion. Based on this information, pore structure parameters, such as pore size distribution and pore volume, can be estimated according to the Washburn theory. Mercury intrusion porosimetry can be further divided into high-pressure mercury injection and constant-speed mercury injection. The differences between these two methods are the mercury injection rate and the maximum mercury injection pressure. The constant-rate mercury intrusion technique is usually conducted at a low injection rate (less than 5×10^{-5} mL/min) and limited injection pressure (maximum pressure is 900 psi) to finely characterize the pore throat information. The maximum pressure of high-pressure mercury injection is fairly higher than that of constant-speed mercury injection. The smallest pore diameter that can be detected using a maximum injection pressure of 60,000 psi is about 3–4 nm. The high-pressure mercury injection is usually applied for characterizing the wide pore size distribution of shales. However, the high-pressure mercury may compress the pores of soft minerals (clays and organic matter in shales) and even create artificial fractures at high-injection pressure conditions. Thus, the pore structure information of shales detected by MIP should be cautiously examined with the aid of other information.

Nitrogen adsorption is especially used for the investigation of nano-scaled pores [48]. Particle or powder samples are vacuumized before the experiment. Then, high-purity nitrogen is used as an adsorbent to adsorb on the pore surface of samples under different relative pressures at −196 °C. Nitrogen adsorption and desorption curves are plotted with the relative pressure as abscissa and adsorption amount as ordinate. The pore size distribution and specific surface area can be interpreted according to the physical adsorption theory [48]. The hysteresis loops, formed by the divergence between the adsorption and desorption branches, are associated with specific pore shapes. The IUPAC (International Union of Pure and Applied Chemistry) divided hysteresis loops into four types [48], as follows. The type H1 hysteresis loop is related to the cylindrical pores with openings at both ends. The type H2 hysteresis loop is always observed in the inkbottle-shaped pores with a thin neck and wide body. The type H3 hysteresis loop is associated with slit-shaped pores or fractures, while the type H4 hysteresis loop is usually related to narrow slit-shaped pores. Previous investigations have shown that the organic matter-hosted pores in shales are constituted by narrow pore throats connecting to large pore bodies [49]. Thus, the wide hysteresis loops (type H2) are always observed in shales with developed organic matter-hosted pores, while the type H3 hysteresis loops are found in pores with clay minerals (plate-like particles) [49,50]. Nitrogen adsorption is widely used to characterize nanoporous materials. However, the effective diffusion coefficients of nitrogen are low (10^{-14}–10^{-12} m^2/s) in micropores at low temperatures [51], which restricts the access of nitrogen to inner pores. This will result in the underestimation of the total pore volume. Moreover, samples for nitrogen adsorption are always crushed into particles that might destroy the authentic pore structure.

Other fluid injection technology, such as water injection and imbibition, is used to not only characterize the pore structure but also increase oil production. Fluid imbibition experiments were conducted to characterize the connectivity of shales according to the time exponent of water imbibition [52]. Low salinity water injection can effectively enhance oil recovery of tight reservoirs by changing rock wettability and reducing interfacial tension [53]. The enhanced oil recovery factor was reported to be up to 14% in carbonate reservoirs using low-salinity water injection [53].

3.3. High-Energy Ray Technology

The high-energy ray technique commonly utilizes X-rays or neutron rays to scan porous materials and then reconstructs minerals and pore phases using three-dimensional imaging technology software. Typical high-energy ray techniques used to characterize the pore space of shales include micro-computed tomography (Micro-CT), nano-computed tomography (Nano-CT), and small-angle neutron scattering. CT scanning recognizes minerals by the differences in the absorption and transmission of X-rays in various minerals and then reconstructs the spatial distribution of minerals using computer algorithms. During the CT scanning, minerals with high density (such as pyrite) appear to be bright-white; minerals with medium density appear to be light-gray (such as quartz, carbonate minerals, and clay minerals); minerals with low density appear to be dark-gray (such as organic matter), while pores appear to be black. Based on the gray-level difference of different components, 3D models of minerals and pores can be reconstructed. The CT scanning yields the three-dimensional spatial structure of minerals and pores, which can be used to evaluate pore connectivity. Zheng et al. used nano-CT to study the pore connectivity of shales from the Ordos Basin (Figure 5) and reported that the average coordination number of the pore network was between 1.34 and 1.84, indicating poor pore connectivity of shales [36].
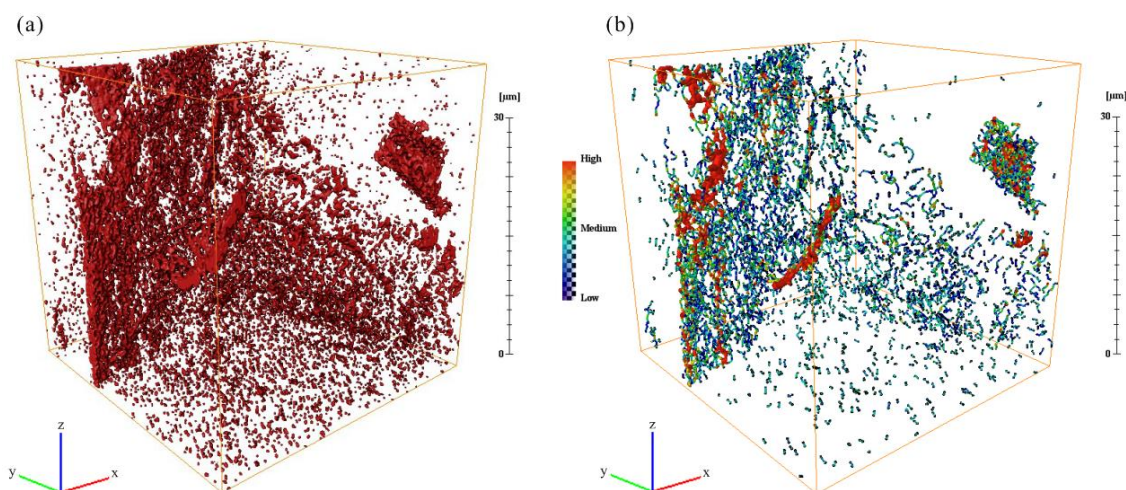

Figure 5. (**a**) Three-dimensional pore and micro-fracture network of the shale from the Ordos Basin detected by Nano-CT scanning; (**b**) Three-dimensional pore connectivity of the shale from the Ordos Basin detected by Nano-CT scanning (modified from Zheng et al. [36]).

When X-rays or neutron beams are introduced to materials, the coherent scattering phenomenon generates in a small-angle range (less than 5°) around the original beam. Small-angle scattering analyzes the coherent scattering caused by the uneven electron density in the materials. At present, small-angle X-ray scattering (SAXS) is an effective tool to study the nano-scaled pores of porous materials. It yields the size, shape, and distribution information, especially pore information of the open and closed pores of the tested samples. Using SAXS, the proportion of closed pores of Longmaxi shales was reported to be up to 42.6% and increased with depth due to the transformation from macropores to micropores [54].

Although there are lots of techniques to characterize the pore structure, pore shapes in shales are very complicated, and pore size distributions span several orders of magnitude from nanometers to micrometers and millimeters. Thus, different techniques are required to perform on the same sample for comparison and supplement. A general experimental procedure for characterizing pore systems in shales is suggested as follows. Firstly, the visually qualitative analyses of pores are conducted by FE-SEM imaging technology. At the same time, the total porosity of shale samples is measured using helium pycnometry. Then,

macropore distributions are evaluated using high-pressure MIP. Mesopore distributions and specific surface areas of shales are obtained using the nitrogen adsorption method. Furthermore, Micro-CT and Nano-CT can be added to characterize the 3D pore structure and pore connectivity. Certainly, the total porosity calculated from the latter should be consistent with the porosity measured using helium pycnometry. Figure 6 illustrates the full-scale pore size distribution of shales from the Ordos Basin, detected using nitrogen adsorption, MIP, and Nano-CT scanning. The dominant pore size of shales from this basin ranges from 10 to 100 nm.
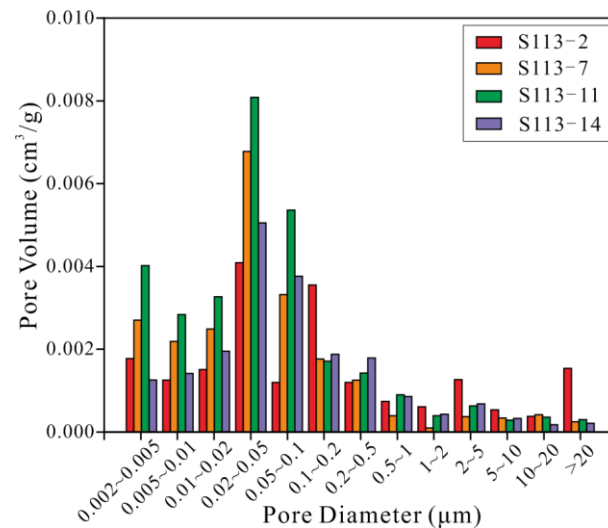
Figure 6. Full-scale pore size distribution of shales from the Ordos Basin, detected using nitrogen adsorption, MIP, and Nano-CT scanning (modified from Zheng et al. [36]).

4. Evaluating Shale Oil Movability

The physical structure of shales affects the movability of shale oil (Figure 7). The CT scanning on tight shales from the Yanchang Formation has shown that the proportion of connected pores is commonly less than 37% [36], indicating that the shale oil movability will be severely restricted. In addition to the pore structure, the movability of shale oil also depends on the interaction between oil and minerals. One of the typical cases is the wettability of pore surfaces. The adsorption layer thickness of shale oil on the hydrophobic surface (e.g., organic matter) is high, thus shale oil will be less movable. Moreover, the hydrocarbon compositions have different adsorption behaviors on mineral surfaces. Asphaltene and resins are thought to tightly adsorb on minerals and restrict shale movability, while shale oil with abundant light hydrocarbons flows easily [55].
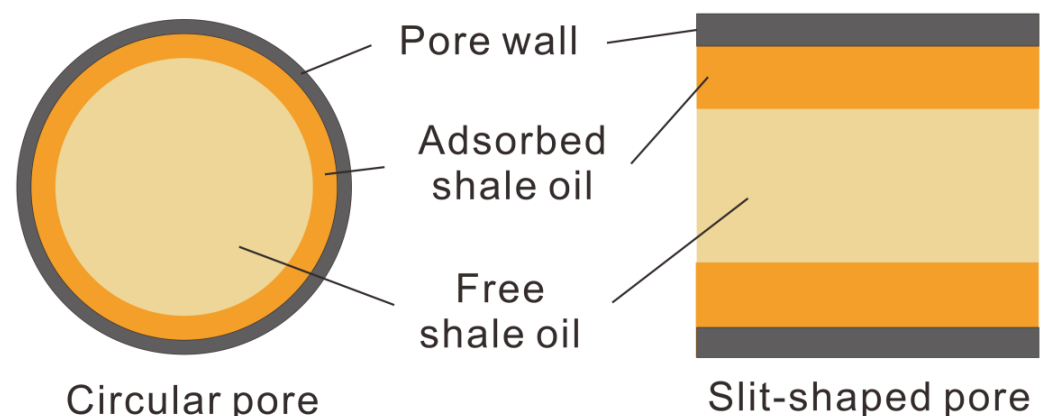

Figure 7. Free and adsorbed shale oil in a circular pore and a slit-shaped pore.

Since the interaction between oil and minerals is complicated, it is difficult to accurately estimate the movability of shale oil. The common technologies estimating the content of free hydrocarbons include the chloroform bitumen "A" extraction, the rock (programmed) pyrolysis technique, and the nuclear magnetic resonance (NMR), etc.

4.1. Rock Pyrolysis

Rock pyrolysis, a method used to evaluate the oil generation potential, is based on the fact that different hydrocarbons have different thermal volatilization capabilities. In rock pyrolysis, light hydrocarbons with small molecular compounds are prone to release at temperatures less than 300 °C and are regarded as free hydrocarbons or free oil (S_1) (Figure 8). The hydrocarbons generated between 300 °C and 650 °C are considered as immobile (S_2). In conventional rock pyrolysis, the S_1 value is regarded as the amount of volatile oil retained in rock, while the S_2 value represents the oil generation potential from kerogen decomposition. However, many studies about source rock geochemistry show that a certain amount of volatile oil is recorded in the S_2 value [23]. In other words, the amount of free oil is probably higher than the S_1 value. Furthermore, the desorbed hydrocarbon from kerogen and the generated hydrocarbon from kerogen decomposition were not clearly differentiated. Recently, a step-by-step rock pyrolysis method was proposed to capture the free oil [56]: the sample is first heated at 200 °C for 1 min to collect the S_{1-1}, and then heated to 350 °C with the heated rate of 25 °C/min to collect the S_{1-2}. Next, the sample is heated to 450 °C to collect the adsorbed oil S_{2-1} and finally heated to 600 °C to collect the oil generation potential from kerogen decomposition S_{2-2}. In step-by-step rock pyrolysis, the sum of S_{1-1} and S_{1-2} is the amount of movable oil, while S_{2-1} represents the adsorbed oil (Figure 8). Several researchers compared the step-by-step rock pyrolysis results of shales before and after extraction with dichloromethane [57]. It was found that the residual amount of S_{1-1} and S_{1-2} was very small after solvent extraction. Most of the adsorbed oil S_{2-1} was extracted, while a small amount of S_{2-2} was extracted. Consequently, they pointed out that the free oil in shales was mainly non-polar and weakly polar compounds, while the adsorbed oil was mostly heavy hydrocarbons, resins, and asphaltene with strong polarity [58].
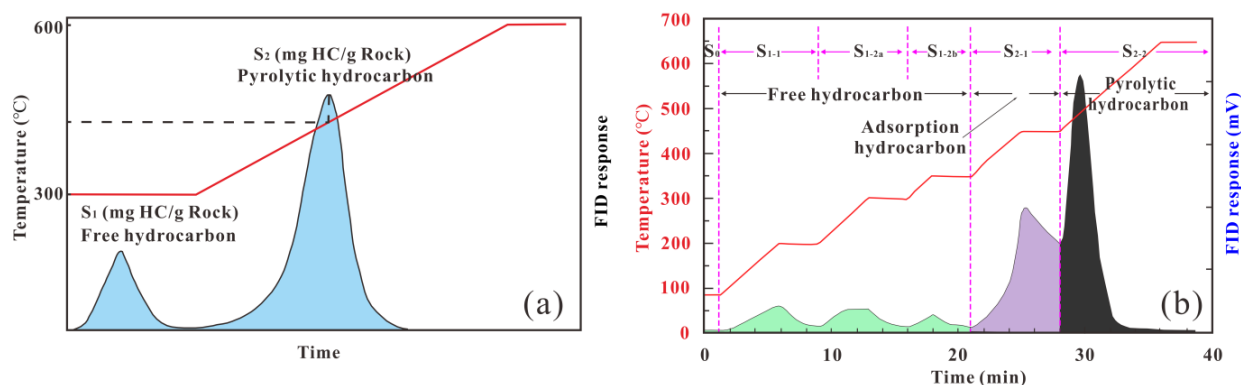
Figure 8. (**a**) Conventional rock pyrolysis and (**b**) step-by-step rock pyrolysis to determine the free, adsorbed, and pyrolytic hydrocarbons of shales.

4.2. Chloroform Bitumen "A" Extraction

Chloroform bitumen "A" refers to the extraction of soluble organic matter from source rocks using chloroform. In this method, the extracted organic matter is considered as movable oil. Shale oil residing in large pores and fractures is easy to be extracted because of its high accessibility with solvents. However, oil residing in micropores is difficult to be extracted due to limited access. It should be noted that the loss of light hydrocarbons cannot be avoided due to evaporation during the chloroform bitumen "A" extraction process. The loss of light hydrocarbons mainly occurs in the following aspects: (1) sample drying, where light hydrocarbons might evaporate when samples are dried

before chloroform extraction; (2) sample crushing, where samples will be heated due to mechanical crushing; (3) extraction loss, Where light hydrocarbons with a boiling point being lower than 200 °C (mainly including the volatile C_1–C_8 organic compounds, [59]) will volatilize during solvent extraction due to the fact that the extraction process is generally conducted at 80 °C. Thus, light hydrocarbon loss is probably serious during this process. In order to accurately determine the amount of light hydrocarbons, Zhu et al. [58] assumed that the composition of produced crude oil from lithologic reservoirs is similar to the retained hydrocarbons in nearby source rocks and found that the recovery coefficient of light hydrocarbons determined from chloroform extraction was between 1.2 and 1.4 when the vitrinite reflectance of source rocks changed from 0.7% to 1.2%. These results indicate that light hydrocarbon loss is probably serious for shale oil at medium-to-high maturity stages.

4.3. Nuclear Magnetic Resonance

Nuclear magnetic resonance (NMR) is a rapid technology to evaluate the content and distribution of fluids. This method detects the relaxation time (T_2) of fluid-saturated and centrifugal samples. The variation of relaxation time before and after centrifugation can be used to calculate the saturation of movable shale oil. In this method, the larger part of the T_2 spectrum distribution represents the movable fluid, while the smaller part of the T_2 spectrum distribution is related to the immovable fluid. Recently, Yan et al. [60] used one-dimensional and two-dimensional NMR to obtain the distribution of free oil and water in lacustrine shale reservoirs. Zhang et al. [24] conducted a series of NMR experiments on shales, clay minerals, and kerogen, and found that the adsorbed shale oil mainly existed in the micropores below 100 nm, while free oil was predominant in the mesopores and macropores (above 100 nm). Nonetheless, several researchers found an abnormal phenomenon whereby the T_2 spectrum of the centrifugal samples is sometimes higher than the fluid-saturated samples [61]. These abnormal T_2 spectrums, likely due to the diffusion between micro-and macro-porosity, no longer accurately represent the pore size and fluid distribution.

5. Geological Controls on Shale Oil Retention and Movability

5.1. Mineral Compositions

Previously, oil retention in source rocks was thought to be primarily related to the organic matter richness, due to the fact that oil can be absorbed by organic matter via adsorption or solvation [28,55]. This can be reflected in the positive relationship between TOC content and S_1 value determined by rock pyrolysis (Figure 9). Based on this, a concept of oil saturation index (OSI = $100 \times S_1/TOC$) was proposed to evaluate the amount of movable oil. Jarvie [28] summarized the shale oil movability of typical source rocks from North America and found that when the OSI value is larger than 100 mg/g TOC, shale oil tends to be moveable. In other words, shale oil will be expelled from source rocks when its amount is large enough for adsorption retention and volumetric storage.

In addition to organic matter, clay minerals also affect shale oil retention. Molecular simulation of shale oil occurrence has found that the density of shale oil on the surface of illite reaches 1.16 g/cm^3, which is lower than that on graphite (1.21 g/cm^3) but higher than the density of free oil (0.75 g/cm^3) [62]. Other researchers measured the hydrocarbon adsorption capacity on minerals and found that the adsorption capacity of asphaltenes on feldspar (7 mg/g) is obviously higher than that on quartz (4.5 mg/g) and calcite (2.16 mg/g) [63,64]. This is attributed to the crystal structure and electric charge of minerals. The double electric layer and electrostatic force of minerals can enhance hydrocarbon adsorption.
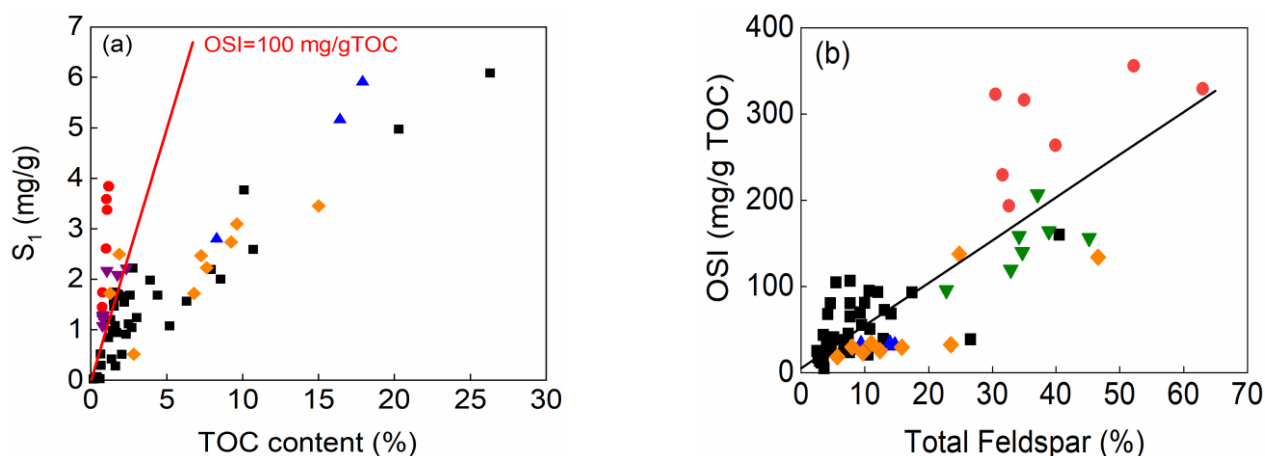
Figure 9. (**a**) The relationship between TOC content and free oil content (S_1); (**b**) The relationship between feldspar content and oil saturation index (OSI = $100 \times S_1/$TOC) for shales from the Ordos Basin (modified from Guo et al. [6]).

5.2. Pore Structure and Pore Size

Pore structure characteristics mainly include pore types, porosity, pore size, surface area, pore connectivity, etc. The bound oil saturation is reported to be partly positive with a specific surface area, which is mainly contributed by small pores [65]. Thus, shale oil will be confined to small pores, while the free oil content is high in large pores. With increasing pore size, the adsorbed layer thickness tends to be constant, and the relative amount of adsorbed oil will decrease.

The inorganic matter pores, like fractures and dissolution-related pores, might be larger than organic matter-hosted pores. Yang et al. [66] measured the pore size distribution of Longmaxi shales and found that although the total porosity of these over-matured shales is controlled by organic matter, shales rich in carbonate minerals have larger pore size distributions than shales rich in organic matter [66]. Some researchers recently reported that the free oil content in shale reservoirs is not always related to the TOC content, but to the development of natural fractures, feldspar content, or biogenic matrices [9,67]. Shale oil retained in these inorganic matter pores (dissolution-related pores, interparticle pores) is thought to be movable and important for shale oil recovery.

5.3. Chemical Compositions of Hydrocarbons

Shale oil consists of aliphatic hydrocarbons, aromatic hydrocarbons, asphaltenes, and resins. The polar components are apt to be adsorbed by organic matter [55]. Thus, the amount of adsorbed oil always increases with the increasing content of asphaltenes and resins. These heavy hydrocarbons tightly adhere to the surface of pores, which decreases shale oil movability. In the future, we will conduct quantitative measurements of the adhesion force of hydrocarbons on typical minerals of shale.

The chemical compositions of hydrocarbons change during petroleum migration and expulsion from source rocks [68]. Petroleum produced from conventional reservoirs is found to be very rich in aliphatic and aromatic hydrocarbons, while the extracted hydrocarbons from source rocks are rich in resins and asphaltenes [69,70]. This geochromatographic effect also exists in shale systems. The geochemical composition analysis of hydrocarbons in "sandwiched" Chang 7 shale systems has shown that polar components are much more abundant in TOC-rich shale intervals than in TOC-lean siltstone intervals [6]. The differences in chemical components of hydrocarbons result in the differential accumulation of oil in complex shale systems.

6. Conclusions

This paper provides a comprehensive review of the present state of knowledge on the occurrence mechanism of liquid hydrocarbons stored in shale systems. We aimed to summarize the various qualitative and quantitative findings related to the occurrence state, occurrence space, content, and oil movability of shale oil. Further, we also provided insights into the moveable shale oil estimation methods and their limitations. The main conclusions are as follows:

1. The image observation technique is suitable for characterizing concentrated pore groups, such as organic matter-hosted pores. The fluid injection technology yields particular pore size information, which should be calibrated using other information. The 3D digital core, demonstrating the spatial distribution of minerals, pores, and pore connectivity, is an effective input for shale oil flow simulation.
2. Inorganic matter pores and fractures are an important occurrence space for shale oil. Due to the low oil adsorption and the high light hydrocarbon content, these inorganic matter pores and fracture networks are probably the "sweet spot" for lacustrine shale systems in China. This contrasts with the previous understanding of oil retention in source rocks.
3. The macro-scaled physical experiments on shale oil movability measure the total free oil content, which neglects the hydrocarbon–rock interactions and the sequential migration of hydrocarbons. The lack of micro-scaled experiments on the interactions between oil and minerals limits the understanding of occurrence mechanisms. This might be resolved by subtly measuring the adhesion forces using an atomic force microscope.
4. Oil intrasource migration in the organic-rich systems affects the chemical composition distribution of hydrocarbons. The superposition effects of multi-scaled pore networks and hydrocarbon–rock interactions complicate shale oil occurrence and migration and further control the "sweet spot" of shale systems. Furthermore, it is necessary to conduct micro-scaled experiments on oil intrasource migration and analyze the results at a molecular level.

Author Contributions: Conceptualization, F.Y.; Data curation, T.B.; Funding acquisition, F.Y.; Investigation, Y.L. (Yangbo Lu), T.B., F.Y. and B.H.; Resources, B.H. and H.G.; Supervision, F.Y.; Validation, H.G.; Visualization, Y.L. (Yongchao Lu); Writing—original draft, Y.L. (Yangbo Lu); Writing—review & editing, F.Y., T.B. and Y.L. (Yongchao Lu). All authors have read and agreed to the published version of the manuscript.

Institutional Review Board Statement: Not applicable.

Informed Consent Statement: Not applicable.

Data Availability Statement: The data presented in this study is available on request from the corresponding author.

Conflicts of Interest: The authors declare no conflict of interest.

References

1. EIA. *Drilling Productivity Report*; U.S. Energy Information Administration: Washington, DC, USA, 2021.
2. Li, Q.Q.; Xu, S.; Zhang, L.; Chen, F.; Wu, S.; Bai, N. Shale Oil Enrichment Mechanism of the Paleogene Xingouzui Formation, Jianghan Basin, China. *Energies* **2022**, *15*, 4038. [CrossRef]
3. Tathed, P.; Han, Y.; Misra, S. Hydrocarbon saturation in upper Wolfcamp shale formation. *Fuel* **2018**, *219*, 375–388. [CrossRef]
4. Ko, L.T.; Loucks, R.G.; Ruppel, S.C.; Zhang, T.; Peng, S. Origin and characterization of Eagle Ford pore networks in the south Texas Upper Cretaceous shelf. *AAPG Bull.* **2017**, *101*, 387–418. [CrossRef]

5. Shao, D.; Zhang, T.; Ko, L.T.; Li, Y.; Yan, J.; Zhang, L.; Luo, H.; Qiao, B. Experimental investigation of oil generation, retention, and expulsion within type II kerogen-dominated marine shales: Insights from gold-tube nonhydrous pyrolysis of Barnett and Woodford Shales using miniature core plugs. *Int. J. Coal Geol.* **2020**, *217*, 1–17. [CrossRef]

6. Guo, Q.L.; Yao, Y.; Hou, L.; Tang, S.; Pan, S.; Yang, F. Oil migration, retention, and differential accumulation in "sandwiched" lacustrine shale oil systems from the Chang 7 member of the Upper Triassic Yanchang Formation, Ordos Basin, China. *Int. J. Coal Geol.* **2022**, *261*, 104077.

7. Liu, B.; Sun, J.; Zhang, Y.; He, J.; Fu, X.; Yang, L.; Xing, J.; Zhao, X. Reservoir space and enrichment model of shale oil in the first member of Cretaceous Qingshankou Formation in the Changling Sag, southern Songliao Basin, NE China. *Pet. Explor. Dev.* **2021**, *48*, 608–624.

8. Li, T.; Liu, B.; Zhou, X.; Yu, H.; Xie, X.; Wang, X.; Rao, H. Classification and evaluation of shale oil enrichment: Lower third member of Shahejie Formation, Zhanhua Sag, Eastern China. *Mar. Petrol. Geol.* **2022**, *143*, 105824. [CrossRef]

9. Zhan, H.; Fang, F.; Li, X.; Hu, Z.; Zhang, J. Shale Reservoir Heterogeneity: A Case Study of Organic-Rich Longmaxi Shale in Southern Sichuan, China. *Energies* **2022**, *15*, 913. [CrossRef]

10. Guo, Q.; Pan, S.; Yang, F.; Yao, Y.; Zheng, H. Characterizing Shale Oil Occurrence in the Yanchang Formation of the Ordos Basin, Assisted by Petrophysical and Geochemical Approaches. *Energy Fuels* **2022**, *36*, 370–381.

11. Lu, S.F.; Huang, W.B.; Chen, F.W.; Li, J.J.; Wang, M.; Xue, H.T.; Wang, W.M.; Cai, X.Y. Classifcation and evaluation criteria of shale oil and gas resources: Discussion and application. *Pet. Explor. Dev.* **2012**, *39*, 249–256. [CrossRef]

12. Zhang, T.; Fu, Q.; Sun, X.; Hackley, P.C.; Ko, L.; Shao, D. Meter-scale lithofacies cycle and controls on variations in oil saturation, Wolfcamp A, Delaware and Midland Basins. *AAPG Bull.* **2012**, *105*, 1821–1846. [CrossRef]

13. Hu, T.; Pang, X.; Jiang, F.; Wang, Q.; Liu, X.; Wang, Z.; Jiang, S.; Wu, G.; Li, C.; Xu, T.; et al. Movable oil content evaluation of lacustrine organic-rich shales: Methods and a novel quantitative evaluation model. *Earth-Sci. Rev.* **2021**, *214*, 103545. [CrossRef]

14. Knapp, L.J.; Ardakani, O.H.; Uchida, S.; Nanjo, T.; Otomo, C.; Hattori, T. The influence of rigid matrix minerals on organic porosity and pore size in shale reservoirs: Upper Devonian Duvernay Formation, Alberta, Canada. *Int. J. Coal Geol.* **2020**, *227*, 103525.

15. Zhang, Y.; Jiang, S.; He, Z.; Li, Y.; Xiao, D.; Chen, G.; Zhao, J. Coupling between Source Rock and Reservoir of Shale Gas in Wufeng-Longmaxi Formation in Sichuan Basin, South China. *Energies* **2021**, *14*, 2679. [CrossRef]

16. Wang, S.; Wang, J.; Zhang, Y.; Li, D.; Jiao, W.; Wang, J.; Lei, Z.; Yu, Z.; Zha, X.; Tan, X. Relationship between Organic Geochemistry and Reservoir Characteristics of the Wufeng-Longmaxi Formation Shale in Southeastern Chongqing, SW China. *Energies* **2021**, *14*, 6716. [CrossRef]

17. Li, Q.; Xu, S.; Hao, F.; Shu, Z.; Chen, F.; Lu, Y.; Wu, S.; Zhang, L. Geochemical characteristics and organic matter accumulation of argillaceous dolomite in a saline lacustrine basin: A case study from the paleogene xingouzui formation, Jianghan Basin, China. *Mar. Pet. Geol.* **2021**, *128*, 105041. [CrossRef]

18. Liu, B.; Wang, H.; Fu, X.; Bai, Y.; Bai, L.; Jia, M.; He, B. Lithofacies and depositional setting of a highly prospective lacustrine shale oil succession from the Upper Cretaceous Qingshankou Formation in the Gulong sag, northern Songliao Basin, northeast China. *AAPG Bull.* **2019**, *103*, 405–432.

19. Bai, C.; Yu, B.; Han, S.; Shen, Z. Characterization of lithofacies in shale oil reservoirs of a lacustrine basin in eastern China: Implications for oil accumulation. *J. Pet. Sci. Eng.* **2020**, *195*, 107907.

20. Hu, S.; Li, S.; Xia, L.; Lv, Q.; Cao, J. On the internal oil migration in shale systems and implications for shale oil accumulation: A combined petrological and geochemical investigation in the Eocene Nanxiang Basin, China. *J. Pet. Sci. Eng.* **2020**, *184*, 106493. [CrossRef]

21. Xu, J.L.; Wang, R.; Zan, L. Shale oil occurrence and slit medium coupling based on a molecular dynamics simulation. *J. Pet. Sci. Eng.* **2023**, *220*, 111151.

22. Sanei, H.; Wood, J.M.; Ardakani, O.H.; Clarkson, C.R.; Jiang, C. Characterization of organic matter fractions in an unconventional tight gas siltstone reservoir. *Int. J. Coal Geol.* **2015**, *150*, 296–305.

23. Li, M.; Chen, Z.; Qian, M.; Ma, X.; Jiang, Q.; Li, Z.; Tao, G.; Wu, S. What are in pyrolysis S_1 peak and what are missed? Petroleum compositional characteristics revealed from programed pyrolysis and implications for shale oil mobility and resource potential. *Int. J. Coal Geol.* **2020**, *217*, 103321.

24. Zhang, P.; Lu, S.; Li, J.; Chang, X. 1D and 2D Nuclear magnetic resonance (NMR) relaxation behaviors of protons in clay, kerogen and oil-bearing shale rocks. *Mar. Petrol. Geol.* **2020**, *114*, 104210. [CrossRef]

25. Donovan, A.; Evenick, J.; Banfield, L.; McInnis, N.; Hill, W. An Organofacies-Based Mudstone Classification for Unconventional tight Rock and Source Rock Plays. In Proceedings of the SPE/AAPG/SEG Unconventional Resources Technology Conference, Austin, TX, USA, 24–26 July 2017.

26. Wang, Q.; Tao, S.; Guan, P. Progress in research and exploration & development of shale oil in continental basins in China. *Nat. Gas Geosci.* **2020**, *31*, 417–427.

27. *GB/T38718-2020*; Geological Evaluation Method for Shale Oil. The Standardization Administration of China: Beijing, China, 2020.

28. Jarvie, D.M. Shale Resource Systems for Oil and Gas: Part 2—Shale-Oil Resource Systems. In *Shale Reservoirs—Giant Resources for the 21st Century*; Breyer, J.A., Ed.; AAPG: Tulsa, OK, USA, 2012; Volume 97, pp. 89–119.

29. Li, T.; Jiang, Z.; Xu, C.; Liu, B.; Liu, G.; Wang, P.; Li, X.; Chen, W.; Ning, C.; Wang, Z. Effect of pore structure on shale oil accumulation in the lower third member of the Shahejie formation, Zhanhua Sag, eastern China: Evidence from gas adsorption and nuclear magnetic resonance. *Mar. Pet. Geol.* **2017**, *88*, 932–949.

30. Han, Y.; Horsfield, B.; Wirth, R.; Mahlstedt, N.; Bernard, S. Oil retention and porosity evolution in organic-rich shales. *AAPG Bull.* **2017**, *101*, 807–827.

31. Matsubara, H.; Umezaki, T.; Funatsu, T.; Tanak, H.; Ikeda, N.; Aratono, M. Thinning and thickening transitions of foam film induced by 2D liquid–solid phase transitions in surfactant–alkane mixed adsorbed films. *Adv. Colloid Interface Sci.* **2020**, *282*, 102206. [CrossRef]

32. Loucks, R.G.; Reed, R.M.; Ruppel, S.C.; Jarvie, D.M. Morphology, genesis, and distribution of nanometer-scale pores in siliceous mudstones of the Mississippian Barnett Shale. *J. Sediment. Res.* **2009**, *79*, 848–861. [CrossRef]

33. Yang, F.; Xu, S.; Hao, F.; Hu, B.; Zhang, B.; Shu, Z.; Long, S. Petrophysical characteristics of shales with different lithofacies in Jiaoshiba area, Sichuan Basin, China: Implications for shale gas accumulation mechanism. *Mar. Petrol. Geol.* **2019**, *109*, 394–407.

34. Milliken, K.L.; Rudnicki, M.; Awwiller, D.N.; Zhang, T. Organic matter-hosted pore system, Marcellus Formation (Devonian), Pennsylvania. *AAPG Bull.* **2013**, *97*, 177–200. [CrossRef]

35. Deng, H.; Hu, X.; Li, H.A.; Luo, B.; Wang, W. Improved pore-structure characterization in shale formations with FESEM technique. *J. Nat. Gas Sci. Eng.* **2016**, *35*, 309–319.

36. Zheng, H.; Yang, F.; Guo, Q.; Pan, S.; Jiang, S.; Wang, H. Multi-scale pore structure, pore network and pore connectivity of tight shale oil reservoir from Triassic Yanchang Formation, Ordos Basin. *J. Petrol. Sci. Eng.* **2022**, *212*, 110283.

37. Mastalerz, M.; Schieber, J. Effect of ion milling on the perceived maturity of shale samples: Implications for organic petrography and SEM analysis. *Int. J. Coal Geol.* **2017**, *183*, 110–119. [CrossRef]

38. Wang, F.; Guo, S. Influential factors and model of shale pore evolution: A case study of a continental shale from the Ordos Basin. *Mar. Petrol. Geol.* **2019**, *102*, 271–282.

39. Laura, F.; Kovscek, A.R. Nano-Imaging of Shale Using Electron Microscopy Techniques. In Proceedings of the SPE/AAPG/SEG Unconventional Resources Technology Conference, Virtual, 20–22 July 2020.

40. Bai, B.; Elgmati, M.; Zhang, H.; Wei, M. Rock characterization of Fayetteville shale gas plays. *Fuel* **2013**, *105*, 645–652. [CrossRef]

41. Zhou, S.; Yan, G.; Xue, H.; Guo, W.; Li, X. 2D and 3D nanopore characterization of gas shale in Longmaxi formation based on FIB-SEM. *Mar. Petrol. Geol.* **2016**, *73*, 174–180. [CrossRef]

42. Huang, C.; Ju, Y.; Zhu, H.; Lash, G.G.; Qi, Y.; Yu, K.; Feng, H.; Ju, L.; Qiao, P. Investigation of formation and evolution of organic matter pores in marine shale by helium ion microscope: An example from the Lower Silurian Longmaxi Shale, South China. *Mar. Petrol. Geol.* **2020**, *120*, 104550.

43. King, H.E.; Eberle, A.P.R.; Walters, C.C.; Kliewer, C.E.; Ertas, D.; Huynh, C. Pore Architecture and Connectivity in Gas Shale. *Energy Fuel* **2015**, *29*, 1375–1390. [CrossRef]

44. Javadpour, F.; Farshi, M.M.; Amrein, M. Atomic-Force Microscopy: A New Tool for Gas-Shale Characterization. *J. Can. Pet. Technol.* **2012**, *51*, 236–243. [CrossRef]

45. Tian, S.; Wang, T.; Li, G.; Sheng, M.; Zhang, P. Nanoscale Surface Properties of Organic Matter and Clay Minerals in Shale. *Langmuir* **2019**, *35*, 5711–5718. [CrossRef]

46. Bai, T.A.; Yang, F.; Wang, H.; Zheng, H. Adhesion Forces of Shale Oil Droplet on Mica Surface with Different Roughness: An Experimental Investigation Using Atomic Force Microscopy. *Energies* **2022**, *15*, 6460. [CrossRef]

47. Wang, K.; Ma, L.; Taylor, K.G. Nanoscale geochemical heterogeneity of organic matter in thermally-mature shales: An AFM-IR study. *Fuel* **2022**, *310*, 122278.

48. Sing, S.K. Reporting physisorption data for gas/solid systems with special reference to the determination of surface area and porosity. *Pure Appl. Chem.* **1985**, *57*, 603–619. [CrossRef]

49. Yang, F.; Ning, Z.; Zhang, R.; Zhao, H.; Krooss, B.M. Investigations on the methane sorption capacity of marine shales from Sichuan Basin, China. *Int. J. Coal Geol.* **2015**, *146*, 104–117. [CrossRef]

50. Yang, F.; Lyu, B.; Xu, S. Water sorption and transport in shales: An experimental and simulation study. *Water Resour. Res.* **2021**, *57*, e2019WR026888.

51. Bertier, P.; Schweinar, K.; Stanjek, H.; Ghanizadeh, A.; Clarkson, C.R.; Busch, A.; Kampman, N.; Prinz, D.; Amann-Hildenbrand, A.; Krooss, B.M.; et al. On the use and abuse of N_2 physisorption for the characterisation of the pore structure of shales. *Clay Miner. Soc. Workshop Lect. Ser.* **2016**, *21*, 151–161.

52. Yang, F.; Zheng, H.; Guo, Q.L.; Lyu, B.; Nie, S.J.; Wang, H. Modeling water imbibition and penetration in shales: New insights into the retention of fracturing fluids. *Energy Fuel* **2021**, *35*, 13776–13787.

53. Khormali, A.; Koochi, M.R.; Varfolomeev, M.A.; Ahmadi, S. Experimental study of the low salinity water injection process in the presence of scale inhibitor and various nanoparticles. *J. Petrol. Explor. Prod. Technol.* **2022**, 1–14. [CrossRef]

54. Sun, M.; Yu, B.; Hu, Q.; Yang, R.; Zhang, Y.; Li, B.; Melnichenko, Y.B.; Cheng, G. Pore structure characterization of organic-rich Niutitang shale from China: Small angle neutron scattering (SANS) study. *Int. J. Coal Geol.* **2018**, *186*, 115–125.

55. Tissot, B.P.; Welte, D.H. *Petroleum Formation and Occurrence*; Springer: Berlin, Germany, 1984.

56. Jiang, Q.; Lim, M.; Qian, M. Quantitative characterization of shale oil in different occurrence states and its application. *Pet. Explor. Dev.* **2016**, *38*, 842–849.

57.　Wang, M.; Ma, R.; Li, J.; Lu, S.; Li, C.; Guo, Z.; Li, Z. Occurrence mechanism of lacustrine shale oil in the Paleogene Shahejie Formation of Jiyang Depression, Bohai Bay Basin, China. *Pet. Explor. Dev.* **2019**, *46*, 789–802.

58.　Zhu, R.F.; Zhang, L.Y.; Li, J.; Liu, Q.; Li, Z.; Wang, R.; Zhang, L. Quantitative evaluation of residual liquid hydrocarbons in shale. *Acta Pet. Sin.* **2015**, *36*, 13–18.

59.　Mango, F.D. The origin of light hydrocarbons. *Geochim. Cosmochim. Acta* **2000**, *64*, 1265–1277. [CrossRef]

60.　Yan, W.; Sun, F.; Sun, J.; Golsanami, N. Distribution Model of Fluid Components and Quantitative Calculation of Movable Oil in Inter-Salt Shale Using 2D NMR. *Energies* **2021**, *14*, 2447. [CrossRef]

61.　Carneiro, G.; Souza, A.; Boyd, A.; Schwartz, L.; Song, Q.; Azeredo, R.; Trevizan, W.; Santos, B.; Rios, E.; Machado, V. Evaluating pore space connectivity by NMR diffusive coupling. In Proceedings of the SPWLA 55th Annual Logging Symposium, Abu Dhabi, United Arab Emirates, 18–22 May 2014.

62.　Wang, Y.; Li, Z.; Wang, M.; Bao, Y.; Zhu, R.; Liu, J.; Wu, L.; Yu, L. Factors controlling lacustrine shale oil adsorption in the Jiyang Depression, Bohai Bay Basin. *Oil Gas Geol.* **2022**, *43*, 489–497.

63.　Ribeiro, R.C.; Correia, J.C.G.; Seidl, P.R. The influence of different minerals on the mechanical resistance of asphalt mixtures. *J. Pet. Sci. Eng.* **2009**, *65*, 171–174. [CrossRef]

64.　Mohammadi, M.; Sedighi, M. Modification of Langmuir Isotherm for the Adsorption of Asphaltene or Resin onto Calcite Mineral Surface: Comparison of Linear and NonLinear Methods. *Physicochem. Processes Interfaces* **2013**, *49*, 460–470. [CrossRef]

65.　Wang, X.; Wang, M.; Li, J.; Shao, H.; Deng, Z.; Wu, Y. Thermal maturity: The controlling factor of wettability, pore structure, and oil content in the lacustrine Qingshankou shale, Songliao Basin. *J. Pet. Sci. Eng.* **2022**, *215*, 110618. [CrossRef]

66.　Yang, F.; Ning, Z.; Wang, Q.; Zhang, R.; Krooss, B. Pore structure characteristics of lower Silurian shales in the southern Sichuan Basin, China: Insights to pore development and gas storage mechanism. *Int. J. Coal Geol.* **2016**, *156*, 12–24. [CrossRef]

67.　Han, Y.; Mahlstedt, N.; Horsfeld, B. The Barnett Shale: Compositional fractionation associated with intraformational petroleum migration, retention, and expulsion. *AAPG Bull.* **2015**, *99*, 2173–2202.

68.　Mahlstedt, N.; Horsfeld, B.; Wilkes, H.; Poetz, S. Tracing the impact of fluid retention on bulk petroleum properties using nitrogen-containing compounds. *Energy Fuel* **2016**, *30*, 6290–6305. [CrossRef]

69.　Leythaeuser, D.; Schaefer, R.G.; Radke, M. Geochemical effects of primary migration of petroleum in Kimmeridge source rocks from Brae feld area, North Sea. I: Gross composition of C_{15+}-soluble organic matter and molecular composition of C_{15+}-saturated hydrocarbons. *Geochim. Cosmochim. Acta* **1988**, *52*, 701–713.

70.　Leythaeuser, D.; Radke, M.; Schaefer, R.G. Efficiency of petroleum expulsion from shale source rocks. *Nature* **1984**, *311*, 745–748. [CrossRef]